Dynamic nuclear polarization of ^{29}Si nuclei in isotopically controlled phosphorus doped silicon

Hiroshi Hayashi, Tatsumasa Itahashi, and Kohei M. Itoh*
School of Fundamental Science and Technology, Keio University, 3-14-1 Hiyoshi, Kohoku-ku, Yokohama 223-8522, Japan

Leonid S. Vlasenko and Marina P. Vlasenko
A. F. Ioffe Physico-Technical Institute, 194021 Saint Petersburg, Russia

(Received 1 January 2009; revised manuscript received 13 May 2009; published 8 July 2009)

Dynamic nuclear polarization (DNP) of ^{29}Si nuclei in isotopically controlled silicon single crystals with the ^{29}Si isotope abundance f_{29Si} varied from 1.2% to 99.2% is reported. It was found that both the DNP enhancement and ^{29}Si nuclear spin-lattice relaxation time under saturation of the electron paramagnetic resonance transitions of phosphorus donors increase with the decrease in the ^{29}Si abundance. A remarkably large steady-state DNP enhancement, $E^{ss}=2680$ which is comparable to the theoretical upper limit of 3310, has been achieved through the "resolved" solid effect that has been identified clearly in the $f_{29Si}=1.2\%$ sample. The DNP enhancement depends not only on the ^{29}Si abundance but also on the electron spin-lattice relaxation time that can be controlled by temperature and/or illumination. The linewidth of ^{29}Si NMR spectra after DNP shows a linear dependence on f_{29Si} for $f_{29Si} \leq 10\%$ and changes to a square-root dependence for $f_{29Si} \geq 50\%$. Comparison of experimentally determined nuclear polarization time with nuclear spin diffusion coefficients indicates that the rate of DNP is limited by the polarization transfer rather than by spin diffusion.

DOI: 10.1103/PhysRevB.80.045201 PACS number(s): 76.70.Fz, 76.30.−v, 28.60.+s, 61.82.Fk

I. INTRODUCTION

Recent proposals of silicon-based spintronic[1] and quantum computing[2–5] devices have activated worldwide efforts in investigation of spin-dependent phenomena in silicon. Realization of silicon spin transistors[1] requires formation of efficient spin injectors on silicon.[6–9] Silicon-based quantum computers require overcoming of technological challenges such as achieving long coherence time of electron[10,11] and nuclear[12] spins, fabrication of appropriate nanostructures,[13] initialization of spins,[14–17] and readout of electron[18] and nuclear[19] spins. Furthermore, it has been shown that the qubit clock speed of at least 10 kHz is needed[20] for practical operation of Shor's factoring algorithm.[21] In this regard electron spins that can be operated much faster than 10 kHz are excellent candidates as quantum processors. However, coherence time of electron spins is typically much shorter than that of nuclear spins. Therefore, there often is the case that nuclear spins are needed as memory qubits that can store information practically forever with implementation of appropriate error correction schemes. Here challenges to be overcome are difficulties in initialization and readout of nuclear spin states.

The present paper describes dynamic nuclear polarization (DNP) experiments to enhance the polarization of ^{29}Si nuclear spins toward efficient initialization needed for nuclear-spin-based silicon quantum computing. DNP induced by the Overhauser effect (OE) and/or the solid effect (SE) is based on the transfer of equilibrium electron polarizations at temperature T and magnetic field B to target nuclear spin systems. The Overhauser effect is driven by saturation of allowed electron paramagnetic resonance (EPR) transitions ($\Delta m_S = \pm 1$, $\Delta m_N = 0$, where m_S and m_N are the electron and nuclear magnetic quantum numbers, respectively), followed by flip-flop relaxation ($\Delta m_S + \Delta m_N = 0$) in electron-nuclear systems coupled by contact hyperfine interaction.[22,23] The solid effect is driven by saturation of forbidden flip-flop and flip-flip transitions ($\Delta m_S + \Delta m_N = \pm 2$) in dipolar-coupled electron-nuclear systems.[23–26] The maximum theoretical value of DNP enhancement E, the ratio of the polarization after DNP P_N to the equilibrium nuclear polarization P_{N0}, is given by $E_{max} = \gamma_e / \gamma_N = 3310$ for silicon,[23] where $\gamma_e = 28$ MHz/mT and $\gamma_N = 8.5$ kHz/mT are the electron and ^{29}Si nuclear gyromagnetic ratios, respectively.

A first series of DNP experiments in silicon was reported by Abragam *et al.*[27] in the context of producing silicon targets for nuclear physics experiments. Using phosphorus doped silicon with a donor concentration $N_d = 5 \times 10^{16}$ cm^{-3}, $E=1200$ and 120 were achieved via the Overhauser effect at 77 K for the resonance frequencies 200 MHz and 9 GHz, respectively.[27] At 4.2 K, the solid effect dominates DNP and $E=30$ corresponding to $P_N = 0.048\%$ was observed under the saturation of the phosphorus EPR lines using 9 GHz.[28] The efficiency of DNP in phosphorus doped silicon at low temperatures is limited by two factors: (i) long electron spin-lattice relaxation time T_{1e} of a phosphorus donor electron that limits the transfer rate of the electron polarization to the nuclear spins[11,29] and (ii) inhomogeneously broadened phosphorus EPR lines in naturally available silicon causing "differential" solid effect.[24,26]

Large E and P_N were achieved with uniaxially stressed boron doped silicon at 1.2 K.[30] DNP employing "integrated" solid effect, which involved reversing electron spin polarization by the application of π microwave pulses or fast adiabatic passage through the inhomogeneously broadened EPR line, lead to a large steady-state DNP enhancement $E^{ss} = 1000$ and DNP degree $P_N^{ss} = 4.4\%$. Note that T_{1e} of boron acceptors is three orders of magnitude shorter than that of phosphorus donors.[31]

Optical nuclear polarization (ONP) of ^{29}Si in bulk silicon was demonstrated by Lampel. Without the application of the

TABLE I. Phosphorus doped silicon samples investigated in this work. The crystal-growth methods [floating zone (FZ) or Czochralski (CZ)], ^{29}Si abundance f_{29Si} (%), ^{29}Si concentration N_N (10^{22} cm^{-3}), phosphorus concentration N_d (10^{15} cm^{-3}), and number of ^{29}Si nuclei per paramagnetic center N_N/N_d are listed.

Sample	Growth	f_{29Si}	N_N	N_d	N_N/N_d
^{29}Si-1%	FZ	1.2	0.06	0.7	8.6×10^5
^{29}Si-5%(10^{15})	CZ	4.7	0.24	0.8	2.9×10^6
^{29}Si-5%(10^{16})	CZ	4.7	0.24	50	4.7×10^4
^{29}Si-5%(10^{17})	CZ	4.7	0.24	500	4.7×10^3
^{29}Si-10%	FZ	10.3	0.52	1.6	3.2×10^6
^{29}Si-50%	FZ	47.9	2.40	0.6	4.0×10^7
^{29}Si-100%	CZ	99.2	4.96	0.8	6.2×10^7

resonant field, Lampel demonstrated ONP of $P_N^{ss}=-0.0002\%$ ($E^{ss}=-5.6$) and $P_N^{ss}=0.0007\%$ ($E^{ss}=28\,000$) by simply illuminating unpolarized and circularly polarized light, respectively, to a *n*-type silicon crystal having $N_d=2\times10^{13}$ cm^{-3} at 77 K.[32] Afterward, the important role of electrons localized at deep levels in the silicon band gap was established by Bagraev and Vlasenko.[33] ONP was shown to be a result of relaxation via forbidden flip-flop and flip-flip transitions of the dipolar-coupled electron-nuclear system. A highly enhanced ONP degree in weak magnetic fields B was obtained because the rate of these transitions is proportional to $1/B^2$. ONP study in silicon has recently been extended to helium temperature and high magnetic field (4.2 K and 7 T) regime and has successfully achieved $P_N^{ss}=0.25\%$.[14]

Photoexcited triplet states (spin $S=1$) of defects in silicon were also employed successfully for efficient DNP and ONP. Nonequilibrium population of magnetic sublevels of triplet centers caused by spin-dependent transitions to the ground singlet state lead to the DNP enhancement many times larger than the maximum enhancement $E_{max}=3310$ expected for the classical DNP mechanisms using spin $S=1/2$ centers. Enhancements of 4000–50 000 were obtained by ONP of silicon using triplet centers.[34] Enhancement of nuclear polarization greater than 7000 was observed in recent DNP experiments using saturation of the EPR transitions of the photoexcited triplet states of radiation defects.[35]

The present study focuses on DNP of ^{29}Si nuclear spins based on saturation of phosphorus donor EPR transitions. A phosphorus EPR spectrum consists of two absorption lines separated by 4.2 mT due to the isotropic hyperfine interaction with the phosphorus nuclear spin $I=1/2$.[36] The hyperfine interaction between an electron bound to a phosphorus donor and a nearby ^{29}Si nucleus (spin $I=1/2$) provides the simplest electron-nuclear spin system to evaluate theoretical models of DNP. ^{29}Si nuclear spins situating around randomly placed phosphorus are polarized by DNP and their spin orientations spread throughout the crystal by spin diffusion between dipolar-coupled ^{29}Si. Isotopic control of the ^{29}Si abundance in bulk silicon[37–39] allows us to change important parameters such as the diffusion barrier d, diffusion radius b, nuclear spin diffusion coefficient D, and the number of nuclei per paramagnetic center N_N/N_d, where N_N is the ^{29}Si concentration. These parameters play important roles in theory of DNP, nuclear spin diffusion, and nuclear spin-lattice relaxation.[23–26,40–42] Linewidths of ^{29}Si NMR and phosphorus EPR depend also on the abundance of ^{29}Si because the dipolar interactions between the lattice ^{29}Si nuclei and between ^{29}Si nuclei and phosphorus paramagnetic centers change with the ^{29}Si abundance. The present study investigates the effects of the ^{29}Si abundance and phosphorus concentration on DNP enhancement and nuclear polarization time of ^{29}Si. The experimental conditions to increase the nuclear polarization are explored by varying the electron spin-lattice relaxation time via temperature and illumination. The discussions toward further improvement of DNP in silicon will be given based on our experimental findings.

II. EXPERIMENTAL

The experiments were performed with phosphorus doped ($N_d\approx10^{15}$ cm^{-3}) isotopically controlled silicon single crystals, whose ^{29}Si abundances f_{29Si} were varied between 1.2% and 99.2%. In parallel, silicon crystals of natural isotopic abundance ($f_{29Si}=4.7\%$) with different phosphorus concentrations $N_d\approx10^{15}-10^{17}$ cm^{-3} were prepared. The sample parameters are summarized in Table I. Growth of the isotopically controlled silicon crystal is described in Refs. 37–39.

A JEOL JES-RE3X X-band continuous-wave EPR spectrometer was used for phosphorus EPR signal detection and for DNP of ^{29}Si lattice isotopes through the saturation of phosphorus EPR lines. A sample placed in a cylindrical TE_{011} mode cavity was cooled with an Oxford Instruments (ESR900) helium gas flow cryostat. The Oxford Instruments temperature controller (503ITC) kept the temperature in the range between 3.2 and 40 K with an accuracy better than $\Delta T=0.1$ K. The first derivative EPR absorption lines were detected using 100 kHz magnetic-field modulation and a lock-in amplifier.

DNP was induced by saturation of a particular EPR transition using the same EPR spectrometer with a maximum microwave power of 200 mW at a fixed microwave frequency of 9 GHz. The magnetic-field modulation amplitude B_m, from 10^{-2} to 1 mT, was optimized for each investigated sample. The time of EPR saturation t was varied between 20 min and 84 h. The DNP experiments were performed in the

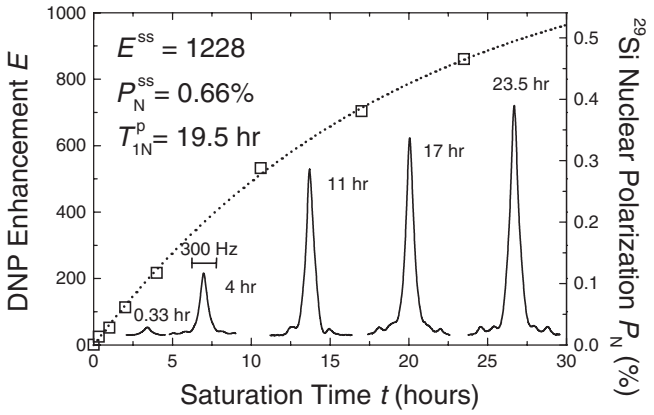

FIG. 1. Dependences of the DNP enhancement E and DNP degree P_N on the saturation time t in ^{29}Si-5%(10^{15}). The dotted line is a single exponential fitting to the experimental data (squares). The inset shows observed ^{29}Si NMR signals. EPR saturation was performed with a modulation amplitude B_m=0.2 mT at 12 K in dark.

dark or under optical excitation with a 1047 nm line from a Nd:YLF-laser.

Upon completion of the saturation in the EPR spectrometer, the sample was warmed up to room temperature and transferred to a Chemagnetics CMX300 CP/MAS-NMR spectrometer. In order to reduce the rapid nuclear relaxation under the weak earth magnetic field,[23] a permanent magnet with the magnetic field of ~10 mT was placed by the sample during the transfer between the EPR and NMR spectrometers. The ^{29}Si NMR signal was detected at room temperature using Fourier-transformed free induction decay after a $\pi/2$ pulse at a magnetic field of 7 T, corresponding to the ^{29}Si NMR frequency of 60 MHz. The pulse length and the acquisition delay time after the $\pi/2$ pulse were 9 and 35 μs, respectively. Long ^{29}Si nuclear spin-lattice relaxation time T_{1N} ranging between 10 min and 3 h at room temperature[43] in comparison with the sample transfer time of ~40 s allowed separation of the EPR saturation and NMR measurements in time and space without a loss of signal intensity.

The value of E, the ratio of P_N to P_{N0}, was determined by comparing the integrated area of the DNP enhanced NMR signal A_{DNP} with the area of the equilibrium NMR signal A_{eq} in accordance with the relation

$$E = \frac{A_{DNP}}{A_{eq}} \frac{T}{300\ \mathrm{K}} \frac{7\ \mathrm{T}}{B}. \quad (1)$$

Here 300 K and 7 T represent the conditions employed for the ^{29}Si NMR measurement while T and B are the temperature and the magnetic field used for saturation in the EPR spectrometer, respectively. The value of P_N was determined by the relation

$$P_N = EP_{N0} = E \tanh\left(\frac{\hbar \gamma_N B}{2k_B T}\right), \quad (2)$$

where $\hbar = h/2\pi$ is the Planck's constant and k_B is the Boltzmann's constant.

A typical experimental dependence of E, P_N, and ^{29}Si NMR signals on saturation duration t is shown in Fig. 1.

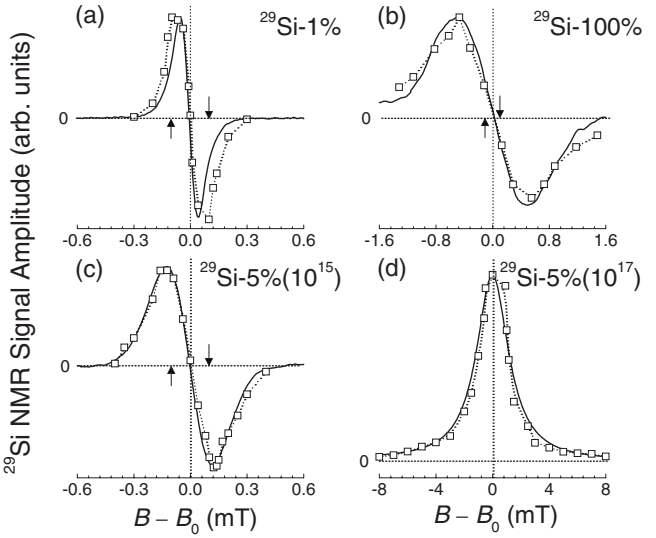

FIG. 2. Comparison of the EPR spectrum (solid curves) and the ^{29}Si NMR signal amplitude (squares) for samples (a) ^{29}Si-1%, (b) ^{29}Si-100%, (c) ^{29}Si-5%(10^{15}), and (d) ^{29}Si-5%(10^{17}). The EPR spectrum for (d) ^{29}Si-5%(10^{17}) is integrated. The NMR signal amplitudes are plotted as a function of the deviation of the magnetic field B from the electron paramagnetic resonant magnetic field B_0 ≈320 mT, $B-B_0$. The positive sign of the ^{29}Si NMR signal amplitude corresponds to the dynamic polarization opposite to the equilibrium ^{29}Si nuclear polarization. The up and down arrows in (a)–(c) indicate the magnetic fields B_0-B_N and B_0+B_N corresponding to the flip-flip and flip-flop transitions of the spin packet placed at B_0, respectively.

Exponential evolution of the nuclear polarization with the saturation time was observed in all the investigated samples. The values of E^{ss}, P_N^{ss}, and nuclear polarization time T_{1N}^{p} (a time constant of the exponential growth) were determined by fitting experimental data (squares) with a single exponential function (dotted line).

III. RESULTS AND DISCUSSIONS

A. Effects of the ^{29}Si and ^{31}P concentrations on DNP enhancement

Identification of the DNP mechanism for different f_{29Si} and N_d was made by comparing the EPR spectrum with the NMR signal amplitude after EPR saturation. The well-known EPR spectrum of phosphorus donors in silicon[36,44] was observed in all investigated samples. All the samples except for ^{29}Si-5%(10^{17}) exhibited a pair of EPR lines separated by 4.2 mT [see Fig. 6(a)]. Each resonance line shown in Figs. 2(a)–2(c) was found to have various peak-to-peak linewidths (PPLWs) ΔB_{pp} ranging between 0.07 and 0.99 mT as listed in Table II. The EPR linewidth dramatically increases with f_{29Si} because the widely extended donor-electron envelope wave function covers a few thousand lattice sites that are randomly occupied by ^{29}Si nuclear spins. A detailed study of phosphorus EPR broadened lines arising from superhyperfine interaction was performed by Abe *et al.*[39] with the same isotopically controlled crystals. Only one broad EPR line due to the strong exchange interaction between the phosphorus

TABLE II. Summary of the result of DNP experiments. PPLW of the first derivative EPR line ΔB_{pp} (mT), mechanisms of DNP [resolved solid effect (RSE) or differential solid effect (DSE) or Overhauser effect (OE)], optimum temperatures for saturation T (K), steady-state DNP enhancement E^{ss}, and steady-state DNP degree P_N^{ss} (%) are listed.

Sample	ΔB_{pp}	DNP	T	E^{ss}	P_N^{ss}
^{29}Si-1%	0.07	RSE	12	2680	1.45
^{29}Si-5%(10^{15})	0.24	DSE	12	1228	0.66
^{29}Si-5%(10^{16})	0.23	DSE	12	511	0.28
^{29}Si-5%(10^{17})	1.55	OE	3.2	−10	−0.02
^{29}Si-10%	0.34	DSE	12	545	0.29
^{29}Si-50%	0.78	DSE	12	787	0.42
^{29}Si-100%	0.99	DSE	12	306	0.17

donors was observed in the relatively high-concentration sample ^{29}Si-5%(10^{17}) [see Figs. 2(d) and 6(b)]. The ^{29}Si NMR signal amplitude measured after 20 min of saturation in the EPR spectrometer at the fixed values of magnetic field B are also plotted in Fig. 2 (squares) as a function of $B-B_0$, where $B_0 \approx 320$ mT is the resonant magnetic field. The saturation was performed in the dark at 3.2 K for ^{29}Si-5%(10^{17}) and at 12 K for the other samples. These temperatures are found to be optimal for DNP as will be discussed in Sec. III C.

The dependence of the amplitude of the DNP enhanced ^{29}Si NMR signal on $B-B_0$ for ^{29}Si-5%(10^{17}) correlates very well with the integrated EPR line as shown in Fig. 2(d). The maximum NMR amplitude was observed for saturation using a magnetic field at the center of the EPR line. This is clear evidence for the Overhauser effect in this highly phosphorus doped sample. For the other samples with $N_d \approx 10^{15}-10^{16}$ cm^{-3}, the dependences of the NMR signal amplitudes on $B-B_0$ correlate very well with the first derivative EPR lines as shown in Figs. 2(a)–2(c) demonstrating that the solid effect is taking place. The maximum ^{29}Si NMR signal amplitudes were observed after the saturation in the EPR spectrometer at magnetic fields corresponding to the peaks of the first derivative EPR lines for the samples with $f_{29Si} \geq 4.7\%$ as shown in Figs. 2(b) and 2(c). However, the saturation magnetic fields which provide maximum NMR amplitudes in ^{29}Si-1% are shifted slightly outside the magnetic fields corresponding to the peak positions of the EPR line [see Fig. 2(a)]. This is clear evidence of the "resolved" solid effect.

The magnetic fields corresponding to the forbidden flip-flop and flip-flip transitions are shifted from the center of the EPR line B_0 by the ^{29}Si nuclear Zeeman frequency, $\pm B_N = \pm B_0(\gamma_N/\gamma_e) = \pm 0.10$ mT. The spacing between the forbidden transitions $2B_N = 0.20$ mT is almost three times larger than the measured PPLW $\Delta B_{pp} = 0.07$ mT for the ^{29}Si-1%, i.e., the maximum NMR amplitudes appear under saturation at $B_0 \pm 0.10$ mT. In other words, isotopic purification of the host crystal by ^{28}Si lead to the elimination of inhomogeneous broadening of the EPR line making it much sharper than $2B_N = 0.20$ mT, i.e., it became possible to resolve the difference in the peak magnetic fields between the EPR spectrum and the dependence of the NMR signal amplitudes on $B-B_0$. This so-called resolved solid effect (RSE) is observed for a first time in silicon. It is also shown that the largest steady-state DNP enhancement $E^{ss}=2680$ was obtained with ^{29}Si-1% for the saturation at $B_0 \pm 0.10$ mT corresponding to the resonant magnetic field of the flip-flop and flip-flip transitions. This value reaches 81% of $E_{max}=3310$ and corresponds to $P_N^{ss}=1.45\%$.

The dependences of the NMR signal amplitude on $B-B_0$ for the other samples resemble the first derivative EPR line. This dependence, nuclear polarization proportional to the first derivative EPR line, shows that DNP is a result of the differential solid effect (DSE). The EPR lines in these samples are inhomogeneously broadened and they are much broader than $2B_N=0.20$ mT. In this case, the microwave field applied at the magnetic field B^* simultaneously saturates the forbidden flip-flop and flip-flip transitions of the different spin packets placed at $B^*[1 \mp (\gamma_N/\gamma_e)]$ leading to the opposite nuclear polarization for the given B^*. The DNP enhancement becomes much smaller than the case for the resolved solid effect. The results of DNP for the condition leading to the largest enhancement for each sample are summarized in Table II. The relatively low E^{ss} in ^{29}Si-10% is due to two times higher phosphorus concentration compared to the other isotopically controlled samples.

The DNP enhancement due to the differential solid effect is reduced from E_{max} and given by[24,26]

$$E(B^*) = -2\xi B^* \left(\frac{dG(B)}{dB} \right)_{B^*}, \tag{3}$$

where ξ is the saturated spin packet width and $G(B)$ is the normalized EPR absorption line-shape function. The parameter ξ can be optimized by applying appropriate magnetic-field modulation $B_m < \Delta B_{pp}$ and using the optimal saturation microwave field B_1 as $\xi \sim (B_1^2+B_m^2+B_i^2)^{1/2}$, where B_i is the intrinsic spin packet width.[24] Under these circumstances, the value of the average slope $\langle dG(B)/dB \rangle$ is inversely proportional to the EPR linewidth. The DNP enhancement E^{ss}/E_{max} corrected for the equal concentration of the phosphorus donors shown in Fig. 3 (squares) correlates very well with the dependence of the inverse EPR PPLW $1/\Delta B_{pp}$ (circles) on f_{29Si}.

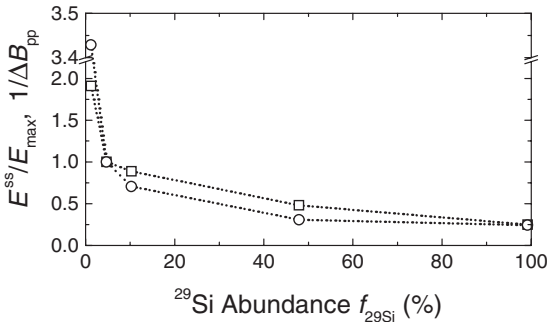

FIG. 3. Dependences of the DNP enhancement E^{ss}/E_{max} corrected for the equal concentration of the phosphorus donors (squares) and the inverse EPR PPLW $1/\Delta B_{pp}$ (circles) on the ^{29}Si abundance f_{29Si} for ^{29}Si-1%, ^{29}Si-5%(10^{15}), ^{29}Si-10%, ^{29}Si-50%, and ^{29}Si-100%. E^{ss}/E_{max} and $1/\Delta B_{pp}$ are normalized by the values of ^{29}Si-5%(10^{15}), respectively.

A two orders of magnitude decrease in E^{ss} with an increase in N_d from 10^{15} to 10^{17} cm^{-3} was observed in the naturally abundant samples (see Table II). This is partly due to the low microwave power (200 mW) that could not saturate completely the EPR line especially when the phosphorus concentration was high. This is also the case for ^{29}Si-50% and ^{29}Si-100% as will be discussed in Sec. III D.

B. ^{29}Si NMR linewidth and nuclear spin diffusion

The NMR spectroscopy allows for investigation of dipolar interactions between ^{29}Si nuclear magnetic moments that affect significantly the coherence and gate operation times of nuclear-spin-based quantum computing. Nuclear spin diffusion among ^{29}Si is especially important for spreading of a particular spin polarization over many spin qubits for initialization.

Nuclear spin diffusion caused by mutual reorientation of two spins in opposite directions (flip-flop transitions) is an important mechanism for expanding the nuclear polarization from paramagnetic centers to the whole crystal volume. It is taken into account in theory of DNP (Refs. 24 and 25) and the equations describing the DNP degree and nuclear polarization time can be simplified significantly when the nuclear spin diffusion time T_{sd} is much shorter than the polarization time of ^{29}Si nuclear spins at the paramagnetic centers. When $T_{sd} \ll T_{1N}^{p}$, so-called average shell-of-influence model[25] is expected to describe the DNP process and T_{sd} is determined by nuclear spin diffusion coefficient D. To verify the applicability of this DNP model, the nuclear spin diffusion coefficient D and the nuclear spin diffusion time T_{sd} were estimated for all investigated silicon crystals containing different concentration of ^{29}Si isotopes. We present this section as an in-depth follow up of our recent preliminary report.[50]

The nuclear spin diffusion coefficient can be described as[26,40]

$$D = a^2 W_{12}, \tag{4}$$

where a is the average distance between two neighboring nuclei and W_{12} is the probability of flip-flop transition. W_{12} can be relatively large for neighboring nuclei and on the order of nuclear spin-spin relaxation rate $1/T_{2N}$, where T_{2N} is the nuclear spin-spin relaxation time. D is described by the following approximate relation:[26]

$$D \approx \frac{1}{30 T_{2N}} a^2 \approx \frac{\Delta \nu_{dd}}{30} a^2, \tag{5}$$

where $\Delta \nu_{dd}$ is the NMR linewidth determined solely by the dipole-dipole interaction between the nuclear magnetic moments. According to the method of moment developed by Van Vleck[45] the linewidth due to dipole-dipole interaction is proportional to the square root of the second moment of Gaussian line shape and to the square root of the magnetic moment concentration. Kittel and Abrahams[46] further derived that the dependence of the linewidth on magnetic-moment concentration is linear for the Lorentzian line shape at low magnetic moment concentration.

Typical DNP enhanced ^{29}Si NMR spectra are shown in Fig. 4. The thermal equilibrium signal for the ^{29}Si-5%(10^{15})

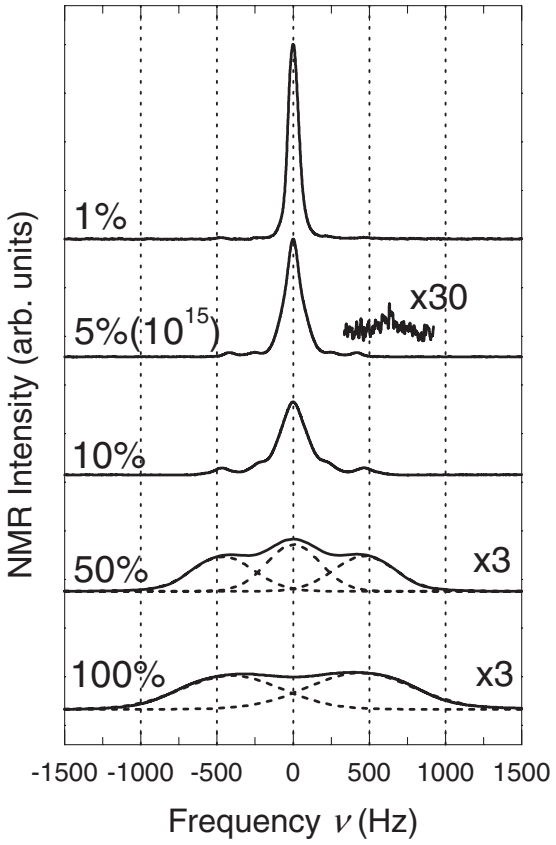

FIG. 4. The DNP enhanced ^{29}Si NMR spectra detected in isotopically controlled silicon single crystals for orientation of the magnetic field approximately along the [111] crystal axis. The horizontal axis is offset by ^{29}Si nuclear Larmor frequency of 60 MHz and the vertical axis is in an arbitrary unit. The thermal equilibrium signal in a ^{29}Si-5%(10^{15}) is also shown (horizontal axis is arbitrarily shifted). The dotted curves in the ^{29}Si-50% and ^{29}Si-100% indicate the components of absorption curves obtained by fitting it with multiple Gaussian curves. The total area under the NMR spectra is normalized to be unity but multiplied to present their shapes clearly.

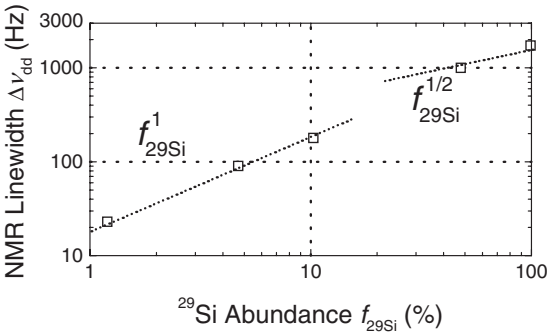

FIG. 5. Dependence of the NMR linewidth due to the dipole-dipole interaction, $\Delta\nu_{dd}$, on the ^{29}Si abundance f_{29Si} for ^{29}Si-1%, ^{29}Si-5%(10^{15}), ^{29}Si-10%, ^{29}Si-50%, and ^{29}Si-100%. The dashed lines show the linear and square-root dependences, respectively.

detected after 66 h relaxation at room temperature and 7 T is also shown to illustrate the effectiveness of DNP. The NMR peaks measured after DNP are strongly enhanced and accompanied by the so-called Pake's doublet arising from the dipole-dipole interaction between the neighbor nuclei and their intensity depends on f_{29Si}.[47–49] The ^{29}Si NMR line shape observed in our samples is Lorentzian for $f_{29Si} \leq 10\%$ and Gaussian for $f_{29Si} \geq 50\%$. Detailed numerical analysis of the line shape based on the method of moment is presented in our recent publication.[50]

To evaluate the linewidths of the complex line shapes, we used the values of $\Delta\nu$ introduced by Myles *et al.*[47] as

$$\Delta\nu = \frac{1}{F(0)}, \tag{6}$$

where $F(0)$ is the value of the normalized NMR line-shape function $F(\nu)$ taken at the center of the NMR line ($\nu = 0$ Hz). It can be seen that the dependence of the NMR linewidths $\Delta\nu$ on f_{29Si} extrapolated to the limit of $f_{29Si}=0\%$ possesses a finite value of ≈ 70 Hz. The residual linewidth of 70 Hz arises from contributions other than the dipolar couplings between the ^{29}Si nuclei, e.g., the inhomogeneity of the external magnetic field over the sample and nonzero delay time of the NMR spectrometer when the strongest part of the free induction decay signal is lost. The residual linewidth of ≈ 70 Hz corresponds to the change in the magnetic field by 0.008 mT and this level of fluctuation can exist in our superconducting magnets operating at 7 T. Verhulst *et al.*[49] have investigated the origin of the similar additional broadening of the ^{29}Si NMR linewidth and attributed to the inhomogenetiy of the external field. The intrinsic dipolar linewidth 93 Hz in ^{29}Si-5%(10^{15}) deduced by subtracting 70 Hz from $\Delta\nu = 163$ Hz shows a reasonable agreement with the PPLW of 0.012 mT, corresponding to 102 Hz, obtained in a continuous-wave ^{29}Si NMR experiment.[48]

To obtain the contribution to the linewidth purely resulting from the dipole-dipole interaction, $\Delta\nu_{dd}$, 70 Hz was subtracted from the $\Delta\nu$ of each sample. The dependence of $\Delta\nu_{dd} = \Delta\nu - 70$ Hz on f_{29Si} obtained in this manner is shown in Fig. 5. This shows a linear dependence on f_{29Si} for $f_{29Si} \leq 10\%$ and approaches a square-root dependence for $f_{29Si} \geq 50\%$. This observation agrees with the theoretical prediction of the linewidth for the system of randomly distributed spins.[47] It was also shown in our recent publication[50] that direct measurement of the full width at half maximum of NMR signal gives similar results.

The nuclear spin diffusion coefficient D can be estimated by substituting the values of $\Delta\nu_{dd}$ and $a \approx N_N^{-1/3}$ into Eq. (5). The time of the nuclear polarization transfer T_{sd} for the half distance between the phosphorus paramagnetic centers $L = R/2$ can be found by

$$T_{sd} \approx \frac{L^2}{D} = \frac{R^2}{4D}, \tag{7}$$

where $R \approx N_d^{-1/3}$ is the average distance between the phosphorus donors. The resulting physical parameters for the nuclear spin diffusion process are summarized in Table III.

Table III shows that the time T_{sd} needed for the lattice ^{29}Si nuclear spins to diffuse a half distance between the phosphorus donors is one order of magnitude shorter than the time T_{1N}^{p} needed to polarize the ^{29}Si nuclear spins situated around each phosphorus. This shows that the nuclear spin polarization (generation) at each phosphorus limits the total spin-polarization rate of ^{29}Si throughout the entire sample. Such condition known as the regime of "rapid nuclear spin diffusion"[42] was confirmed for all the samples. It also indicates that nuclear spin polarization is spatially homogeneous throughout the entire sample during the DNP process and the

TABLE III. Summary of the physical parameters for the nuclear spin diffusion process. The average distance between ^{29}Si nuclei a (Å), average half distance between phosphorus donors L (Å), nuclear spin diffusion coefficient D (10^{-14} cm^2/s), nuclear spin diffusion time T_{sd} (h), and nuclear polarization time T_{1N}^{p} (h) are listed.

Sample	a	L	D	T_{sd}	T_{1N}^{p}
^{29}Si-1%	12	560	1.1	0.82	73.5
^{29}Si-5%(10^{15})	7.5	540	1.7	0.47	19.5
^{29}Si-5%(10^{16})	7.5	140	1.7	0.03	1.2
^{29}Si-5%(10^{17})	7.5	63	1.7	0.006	0.11
^{29}Si-10%	5.8	430	2.0	0.25	4.5
^{29}Si-50%	3.5	590	4.0	0.24	8.8
^{29}Si-100%	2.7	540	4.3	0.19	9.3

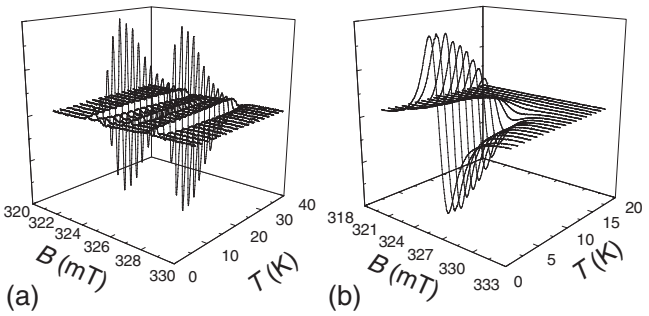

FIG. 6. Variation in the phosphorus EPR spectrum with temperature in (a) ^{29}Si-5%(10^{16}) and (b) ^{29}Si-5%(10^{17}). The microwave power was fixed at 1 mW for all the measurements.

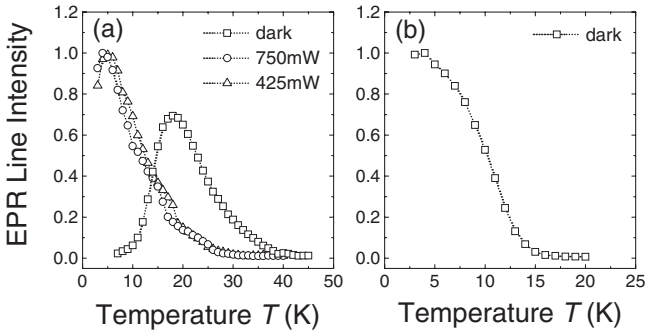

FIG. 7. Temperature dependence of the EPR line intensity in (a) ^{29}Si-5%(10^{16}) and (b) ^{29}Si-5%(10^{17}). The intensities of the EPR line detected in dark (squares), under illumination with Nd:YLF-laser power of 750 mW (circles), and 425 mW (triangles) are shown. The microwave power was fixed at 1 mW in all the measurements.

average shell-of-influence model[24,25] that considers the average interaction between each paramagnetic center and the many surrounding nuclei is applicable.

C. Effects of temperature and illumination on DNP enhancement

The transfer of the equilibrium electron polarization to the ^{29}Si nuclear spin system depends on T_{1e} because each electron spin must typically flip N_N/N_d times together with the surrounding nuclear spins to polarize all the ^{29}Si nuclei between the paramagnetic centers. The closer the electron polarization is to the equilibrium Boltzmann polarization established in the time scale T_{1e}, the stronger the nuclear polarization becomes during the DNP process. Taking into account such an effect the leakage factor f_L can be described as[24]

$$f_L = \frac{N_N T_{1e}}{N_d T_{1N}}. \tag{8}$$

Here, T_{1N} is the nuclear spin-lattice relaxation time without saturation of the forbidden flip-flop and flip-flip transitions. T_{1N} was not measured in this study because it can be more than 100 h at helium temperatures for the samples having $N_d \approx 10^{15}$ cm^{-3}. DNP enhancement is reduced by the factor $(1+f_L)^{-1}$ for the high saturation level of the forbidden EPR transitions,[24]

$$E^{ss} = E_{max}\left(\frac{1}{1+f_L}\right). \tag{9}$$

For the isotopically controlled samples f_L can be estimated by taking the ratio N_N/N_d, which depends on f_{29Si}, T_{1e}, and T_{1N}. Using $N_N/N_d \sim 10^7$, $T_{1e} \sim 10$ s for 4.2 K and $\sim 10^{-4}$ s for 12 K (Refs. 11 and 29) and the temperature independent $T_{1N} \sim 10^6$ s, we find $f_L \sim 100$ for 4.2 K and $f_L \sim 10^{-3}$ for 12 K. While the present analysis is only an estimation, the strong dependence of T_{1e} on the temperature is the major contribution to the temperature dependence of f_L and DNP enhancement.

Temperature dependence of the phosphorus EPR spectrum of ^{29}Si-5%(10^{16}) is shown in Fig. 6(a). The maximum EPR intensity was observed at a temperature around 18 K. The decreases in the EPR intensity for $T > 25$ K and $T < 15$ K are due to thermal ionization of the phosphorus donors and the extension of the electron spin-lattice relaxation time, respectively. Similar temperature dependences were observed with all the samples except for the highly phosphorus doped ^{29}Si-5%(10^{17}) that shows a single EPR line signal gradually decreasing with the increase in the temperature [see Fig. 6(b)].

Figure 7(a) shows the comparison of the temperature dependence of the EPR intensity with and without the band-gap illumination for ^{29}Si-5%(10^{16}). Similar temperature dependences were confirmed in all other samples exhibiting the solid effect. It is well known that the photoexcitation of electrons to the conduction band by the band-gap illumination reduces T_{1e} of the localized electrons by several orders of magnitude.[29] T_{1e} shortened by the spin exchange between the photoexcited conduction electrons and donor electrons leads to an increase in the phosphorus EPR intensity below 10 K. Figure 7(b) shows the temperature dependence of the single EPR line intensity in ^{29}Si-5%(10^{17}) in the dark. Here the illumination has very little effect because of existence of the high-density carriers leading to short T_{1e} even in the dark.

Temperature dependence of E^{ss} was also studied. The saturation for each sample was performed at a magnetic field corresponding to the maximum amplitude of the NMR signal in Fig. 2. Figure 8(a) shows the temperature dependence of E^{ss} for ^{29}Si-5%(10^{16}). Similar temperature dependences were confirmed for all the samples exhibiting the solid effect. These dependences correlate very well with that of the EPR line intensities as can be seen by comparing Fig. 8(a) with Fig. 7(a). The temperature dependence of E^{ss} for ^{29}Si-5%(10^{17}) exhibiting the Overhauser effect is also similar to that of the EPR intensity as can be seen by comparing Fig. 8(b) with Fig. 7(b). The maximum values of E^{ss} were achieved at 12 K without illumination in the samples exhibiting the solid effect. The decrease in E^{ss} at lower temperatures is due to the increase in T_{1e} and consequently to the increase in f_L. This explains the low enhancement $E=30$ obtained in the earlier experiments performed by Abragam *et al.*[28] at 4.2 K. Shortening of T_{1e} by the illumination leads to an increasing of dynamic polarization even in the low-temperature region. The maximum value of $E^{ss}=-10$ was

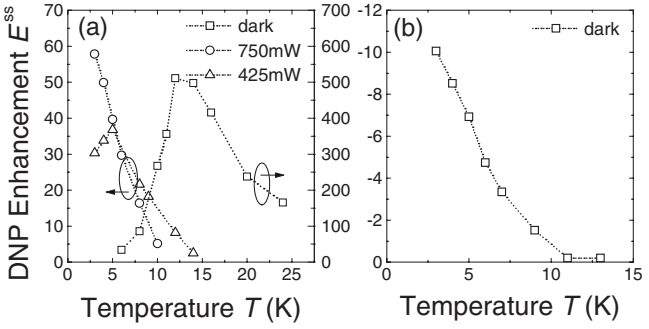

FIG. 8. Temperature dependence of the steady-state DNP enhancement E^{ss} in (a) ^{29}Si-5%(10^{16}) and (b) ^{29}Si-5%(10^{17}). E^{ss} in the dark (squares), under illumination with Nd:YLF-laser power of 750 mW (circles), and 425 mW (triangles) are shown. The left and right axes in (a) correspond to E^{ss} under illumination and in the dark, respectively.

obtained at 3.2 K in the dark for ^{29}Si-5%(10^{17}) that exhibits the Overhauser effect.

D. Effect of the ^{29}Si and ^{31}P concentrations on the nuclear polarization time

Similar to the results of the ^{13}C DNP experiments in the diamond,[51] the linear dependence of the nuclear polarization rate $1/T_{1N}^{p}$ on N_d was found for naturally abundant silicon samples investigated in this study. However, nonmonotonous behavior of $1/T_{1N}^{p}$ on f_{29Si} was found. The dependence of $1/T_{1N}^{p}$ that has been scaled to the value for the donor concentration $N_d=10^{15}$ cm^{-3} is shown in Fig. 9 (squares). $1/T_{1N}^{p}$ increases linearly with f_{29Si} for $f_{29Si}\leq 10\%$, while $1/T_{1N}^{p}$ saturates and decreases with an increase in f_{29Si} for $f_{29Si}\geq 50\%$. The linear dependence for $f_{29Si}\leq 10\%$ is in accordance with theory of nuclear spin-lattice relaxation. Its deviation for $f_{29Si}\geq 50\%$ is due to incomplete saturation of the forbidden transitions.

$1/T_{1N}^{p}$ depends on the nuclear spin diffusion processes, microwave power employed in saturation, and the leakage factor. One order of magnitude difference in $1/T_{1N}^{p}$ between

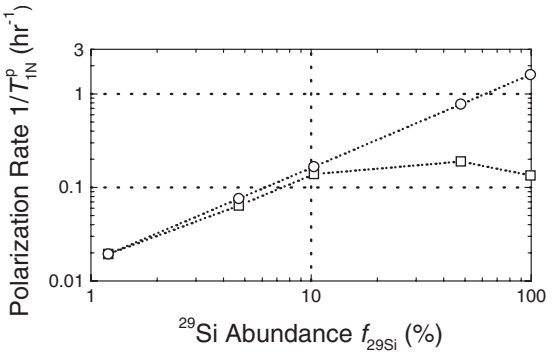

FIG. 9. Dependences of the nuclear polarization rate $1/T_{1N}^{p}$ scaled to be the value at the donor concentration $N_d=10^{15}$ cm^{-3} (squares), and the nuclear polarization rate assuming complete saturation and the absence of extraneous nuclear relaxation (circles). The latter rate is scaled to have the same value as the former rate at $f_{29Si}=1.2\%$.

^{29}Si-1% and ^{29}Si-10% cannot be explained by the factor of 2 increase in D (see Table III). In the regime of rapid nuclear spin diffusion, the average shell-of-influence model[25] can be applied with a nuclear spin-lattice relaxation rate $1/T_{1N}$ without EPR saturation,

$$\frac{1}{T_{1N}}=\frac{3}{10}\left(\frac{g\beta}{B}\right)^2\frac{1}{T_{1e}}\frac{N_d}{d^3}=C\frac{N_d}{d^3}, \tag{10}$$

where g is the electron g factor, β is the Bohr magnetron, and d is the diffusion barrier. d is defined as the distance at which the magnetic field of the paramagnetic center is equal to the dipole field of the nearest nucleus[25,26,42]

$$\left(\frac{\mu_e B}{k_B T}\right)\left(\frac{\mu_e}{d^3}\right)\approx\frac{\mu_N}{a^3}, \tag{11}$$

where μ_e and μ_N are the electron and nuclear magnetic moments, respectively. The case of rapid nuclear spin diffusion corresponds to $d>b$, where b is the diffusion radius given as[26,41,42]

$$b=0.68\left(\frac{C}{D}\right)^{1/4}. \tag{12}$$

Here, b gives the distance from the paramagnetic center at which the nucleus has an equal probability of being flipped by the paramagnetic center or by a neighboring nucleus. In the diffusion-limited case corresponding to $d<b$, $1/T_{1N}$ is given by[26,41,42]

$$\frac{1}{T_{1N}}=4\pi N_d b D=8.5N_d C^{1/4}D^{3/4}. \tag{13}$$

The nuclear polarization rate $1/T_{1N}^{p}$ is faster than the nuclear spin-lattice relaxation rate $1/T_{1N}$ without EPR saturation. If the saturation is sufficient, $1/T_{1N}^{p}$ depends on f_L, according to the relation[24]

$$\frac{1}{T_{1N}^{p}}=\frac{1}{T_{1N}}\left(\frac{1+f_L}{f_L}\right). \tag{14}$$

Two cases are considered. First, if the extraneous nuclear relaxation is significant f_L is proportional to N_N/N_d (Ref. 24) and, consequently, to f_{29Si}. According to Eq. (14) $1/T_{1N}^{p}$ is inversely proportional to f_L for $f_L\ll 1$ and approaches $1/T_{1N}$ for $f_L\gg 1$. This behavior is clearly inconsistent with our experimental results. In the second case, if the extraneous nuclear relaxation is negligibly small, the leakage factor becomes $f_L\ll 1$ and does not depend on N_N/N_d.[24] In this simple case, $1/T_{1N}^{p}$ is proportional to $1/T_{1N}$ and therefore depends linearly on $d^{-3}\sim a^{-3}\sim f_{29Si}$ according to Eq. (10). Such a linear dependence passing an experimentally found $1/T_{1N}^{p}$ value for $f_{29Si}=1.2\%$ shown in Fig. 9 describes the linear increase in $1/T_{1N}^{p}$ for $f_{29Si}\leq 10\%$ very well. The dependence of D on f_{29Si} appearing in Eq. (13) is too weak to explain the experimentally observed increase in $1/T_{1N}^{p}$. Deviation of the experimentally observed nuclear polarization rate from the linear dependence for $f_{29Si}\geq 50\%$ may be attributed to the incomplete saturation of forbidden transitions. In the case of an inhomogeneously broadened EPR line, only a small part of the ensemble of spin packets can be saturated and the

remaining spin packets contribute to the leakage of the nuclear polarization.

It is not possible to determine the values of f_L without the knowledge of $1/T_{1e}$ and $1/T_{1N}$. It requires measurements of extremely long T_{1N} that reaches several days at low temperatures. The leakage factor estimated by Eq. (9) is $f_L \approx 0.235$ using the experimental value of $E^{ss}=2680$ for ^{29}Si-1%. This value should be regarded as an upper limit for f_L because the forbidden transitions overlap partially with the EPR lines, as shown in Fig. 2(a), and such an overlap decreases the DNP enhancement. Using Eq. (14) we can estimate the lower limit of the nuclear spin-lattice relaxation time as $T_{1N} \approx 386$ h for ^{29}Si-1%.

E. Toward further improvement of DNP in silicon

Thanks to the resolved solid effect, we have achieved the DNP enhancement that is close to the theoretical limit with ^{29}Si-1%. Lower enhancements in other samples showing the differential solid effect can be improved significantly by applying the integrated solid effect.[30] On the other hand increasing the magnetic field up to a few tesla will lead to resolved solid effect even in the higher ^{29}Si samples because the spacing between the forbidden transitions is given by $2B_N$.

Very long electron spin-lattice relaxation time of the low-density phosphorus samples at around 4 K is revealed to be limiting the DNP enhancement. Because such low temperature is needed for large polarization, the long electron spin-lattice relaxation time must be shortened. However, our attempt of DNP under illumination or with higher phosphorus doping to shorten the relaxation time did not only work but even reduced the enhancement significantly. The DNP enhancement depends strongly on the maximum power of microwave source for such high carrier density samples. Indeed, high microwave power irradiation under very low temperature was employed recently and the DNP enhancement of $E=150$ corresponding to $P_N=5\%$ was obtained for silicon microparticles at 1.4 K and 2.35 T.[16] DNP of our bulk samples with such high power microwave should lead to larger enhancements.

By far the simplest approach to achieve higher nuclear polarizations is seeking for higher magnetic fields and lower temperature. Recently, 68% polarization of ^{31}P nuclear spins in silicon has been obtained at 1.37 K and 8.5 T without resonant manipulation.[17] However, quantum computing scheme very often requires moderate temperature, magnetic field, and irradiation powers in order to optimize all the other elements such as logic operation and readout processes. In this regards, it is worthwhile to employ other paramagnetic centers having shorter electron spin-lattice relaxation time, for example, boron, lithium, etc., to seek for higher DNP of ^{29}Si nuclei.

IV. CONCLUSION

We have investigated EPR-induced DNP of ^{29}Si in silicon single crystals containing controlled concentrations of phosphorus donors and ^{29}Si isotopes. The Overhauser effect was observed in the sample with phosphorus concentration $N_d \approx 10^{17}$ cm^{-3} due to the electron exchange between the phosphorus donors. The solid effect via fixed phosphorus paramagnetic centers was observed in the samples with lower phosphorus concentrations $N_d \approx 10^{15}-10^{16}$ cm^{-3}. The largest DNP enhancement $E^{ss}=2680$ corresponding to 81% of $E_{max}=3310$ and $P_N^{ss}=1.45\%$ was observed in the sample with least amount (1.2%) of ^{29}Si. This is a result of the sharp EPR line exhibiting the resolved solid effect allowing for the selective saturation of the forbidden transition. The DNP enhancement in samples with larger ^{29}Si concentrations is due to a differential solid effect and decreases with increasing ^{29}Si concentrations.

The DNP enhancement depends strongly on the electron spin-lattice relaxation time T_{1e} which was controlled successfully by temperature and illumination. The temperature dependence of E^{ss} correlates very well with that of the EPR line intensity. The maximum DNP enhancement without illumination was observed at 3.2 K for the sample exhibiting the Overhauser effect and at 12 K for the samples exhibiting the solid effect.

The linewidth of DNP enhanced ^{29}Si NMR peaks is proportional to the ^{29}Si isotope abundance f_{29Si} for $f_{29Si} \leq 10\%$ and approaches square-root dependence for $f_{29Si} \geq 50\%$. The spin diffusivity D for room temperature obtained from the NMR linewidth varied between 1×10^{-14} cm^2/s for $f_{29Si}=1.2\%$ and 4×10^{-14} cm^2/s for $f_{29Si}=99.2\%$. The comparison of the nuclear polarization time T_{1N}^p with the nuclear spin diffusion time T_{sd} shows that $T_{sd} \ll T_{1N}^p$ for all of the investigated samples, i.e., the regime of rapid nuclear spin diffusion takes place.

The dependence of the nuclear polarization rate $1/T_{1N}^p$ was found to be proportional to N_d. $1/T_{1N}^p$ was also proportional to f_{29Si} for $f_{29Si} \leq 10\%$. The linear increase in $1/T_{1N}^p$ with f_{29Si} is explained by a decrease in the distance between the ^{29}Si nuclei and diffusion barrier, rather than by the increase in D with the increase in f_{29Si}. The deviation from the linear dependence for $f_{29Si} \geq 50\%$ is attributed to the incomplete saturation of forbidden transitions.

ACKNOWLEDGMENTS

The authors thank the Central Service Facilities for Research at Keio University for the provision of the well-developed experimentation environment. We thank Wonhee Ko and Naoki Isogai for the technical assistance and Eisuke Abe for helpful discussions. This work was supported in part by Grant-in-Aid for Scientific Research by MEXT Specially Promoted Research No. 18001002, by Special Coordination Funds for Promoting Science and Technology, by JST-DFG Strategic Cooperative Program on Nanoelectronics, and by Grant-in-Aid for the Global Center of Excellence at Keio University.

*kitoh@appi.keio.ac.jp

[1] S. Sugawara and M. Tanaka, Appl. Phys. Lett. **84**, 2307 (2004).
[2] B. K. Kane, Nature (London) **393**, 133 (1998).
[3] T. D. Ladd, J. R. Goldman, F. Yamaguchi, Y. Yamamoto, E. Abe, and K. M. Itoh, Phys. Rev. Lett. **89**, 017901 (2002).
[4] K. M. Itoh, Solid State Commun. **133**, 747 (2005).
[5] J. Gorman, D. G. Hasko, and D. A. Williams, Phys. Rev. Lett. **95**, 090502 (2005).
[6] B.-C. Min, K. Motohashi, C. Lodder, and R. Jansen, Nature Mater. **5**, 817 (2006).
[7] B. Huang, D. J. Monsma, and I. Appelbaum, Phys. Rev. Lett. **99**, 177209 (2007).
[8] I. Appelbaum, B. Huang, and D. J. Monsma, Nature (London) **447**, 295 (2007).
[9] B. T. Jonker, G. Kioseoglou, A. T. Hanbicki, C. H. Li, and P. E. Thompson, Nat. Phys. **3**, 542 (2007).
[10] E. Abe, K. M. Itoh, J. Isoya, and S. Yamasaki, Phys. Rev. B **70**, 033204 (2004).
[11] A. M. Tyryshkin, S. A. Lyon, A. V. Astashkin, and A. M. Raitsimring, Phys. Rev. B **68**, 193207 (2003).
[12] T. D. Ladd, D. Maryenko, Y. Yamamoto, E. Abe, and K. M. Itoh, Phys. Rev. B **71**, 014401 (2005).
[13] T. Sekiguchi, S. Yoshida, and K. M. Itoh, Phys. Rev. Lett. **95**, 106101 (2005).
[14] A. S. Verhulst, I. G. Rau, Y. Yamamoto, and K. M. Itoh, Phys. Rev. B **71**, 235206 (2005).
[15] H. Hayashi, W. Ko, T. Itahashi, A. Sagara, K. M. Itoh, L. S. Vlasenko, and M. P. Vlasenko, Phys. Status Solidi C **3**, 4388 (2006).
[16] A. E. Dementyev, D. G. Cory, and C. Ramanathan, Phys. Rev. Lett. **100**, 127601 (2008).
[17] D. R. McCamey, J. van Tol, G. W. Morley, and C. Boehme, Phys. Rev. Lett. **102**, 027601 (2009).
[18] B. E. Kane, N. S. McAlpine, A. S. Dzurak, R. G. Clark, G. J. Milburn, H. B. Sun, and H. Wiseman, Phys. Rev. B **61**, 2961 (2000).
[19] A. Yang, M. Steger, D. Karaiskaj, M. L. W. Thewalt, M. Cardona, K. M. Itoh, H. Riemann, N. V. Abrosimov, M. F. Churbanov, A. V. Gusev, A. D. Bulanov, A. K. Kaliteevskii, O. N. Godisov, P. Becker, H.-J. Pohl, J. W. Ager, and E. E. Haller, Phys. Rev. Lett. **97**, 227401 (2006).
[20] R. Van Meter and K. M. Itoh, Phys. Rev. A **71**, 052320 (2005).
[21] L. J. Schulman and U. Vazirani, Proceedings of the 31st ACM Symposium on Theory of Computing, 1999 (unpublished), p. 322; D. E. Chang, L. M. Vandersypen, and M. Steffen, Chem. Phys. Lett. **338**, 337 (2001).
[22] A. W. Overhauser, Phys. Rev. **92**, 411 (1953).
[23] A. Abragam, *The Principles of Nuclear Magnetism* (Oxford University Press, New York, 1961).
[24] O. S. Leifson and C. D. Jeffries, Phys. Rev. **122**, 1781 (1961).
[25] T. J. Schmugge and C. D. Jeffries, Phys. Rev. **138**, A1785 (1965).
[26] G. R. Khutsishvili, Sov. Phys. Usp. **8**, 743 (1966).
[27] A. Abragam, J. Combrisson, and I. Solomon, Compt. Rend. **246**, 1035 (1958).
[28] A. Abragam, J. Combrisson, and I. Solomon, Compt. Rend. **247**, 2337 (1958).
[29] G. Feher and E. A. Gere, Phys. Rev. **114**, 1245 (1959).
[30] A. Henstra, P. Dirksen, and W. Th. Wenckebach, Phys. Lett. A **134**, 134 (1988).
[31] P. Dirksen, A. Henstra, and W. Th. Wenckebach, J. Phys.: Condens. Matter **1**, 8535 (1989).
[32] G. Lampel, Phys. Rev. Lett. **20**, 491 (1968).
[33] N. T. Bagraev and L. S. Vlasenko, Sov. Phys. JETP **48**, 878 (1978).
[34] L. S. Vlasenko, M. P. Vlasenko, V. N. Lomasov, and V. A. Khramtsov, Sov. Phys. JETP **64**, 612 (1986).
[35] L. S. Vlasenko, M. P. Vlasenko, D. S. Poloskin, R. Laiho, H. Hayashi, T. Itahashi, A. Sagara, and K. M. Itoh, Phys. Status Solidi C **3**, 4376 (2006).
[36] G. Feher, Phys. Rev. **114**, 1219 (1959).
[37] K. Takyu, K. M. Itoh, K. Oka, N. Saito, and V. I. Ozhogin, Jpn. J. Appl. Phys., Part 2 **38**, L1493 (1999).
[38] K. M. Itoh, J. Kato, M. Uemura, A. K. Kaliteevskii, O. N. Godisov, G. G. Devyatych, A. D. Bulanov, A. V. Gusev, I. D. Kovalev, P. G. Sennikov, H.-J. Pohl, N. V. Abrosimov, and H. Riemann, Jpn. J. Appl. Phys., Part 1 **42**, 6248 (2003).
[39] E. Abe, A. Fujimoto, J. Isoya, S. Yamasaki, and K. M. Itoh, arXiv:cond-mat/0512404 (unpublished).
[40] N. Bloembergen, Physica **15**, 386 (1949).
[41] P. G. de Gennes, J. Phys. Chem. Solids **7**, 435 (1958).
[42] W. E. Blumberg, Phys. Rev. **119**, 79 (1960).
[43] R. G. Shulman and B. J. Wyluda, Phys. Rev. **103**, 1127 (1956).
[44] S. Maekawa and N. Kinoshita, Jpn. J. Appl. Phys. **20**, 1447 (1965).
[45] J. H. Van Vleck, Phys. Rev. **74**, 1168 (1948).
[46] C. Kittel and E. Abrahams, Phys. Rev. **90**, 238 (1953).
[47] C. W. Myles, C. Ebner, and P. A. Fedders, Phys. Rev. B **14**, 1 (1976).
[48] L. S. Vlasenko, N. V. Zavaritskii, S. V. Sorokin, and V. G. Fleisher, Zh. Eksp. Teor. Fiz. **91**, 1496 (1986).
[49] A. S. Verhulst, D. Maryenko, Y. Yamamoto, and K. M. Itoh, Phys. Rev. B **68**, 054105 (2003).
[50] H. Hayashi, K. M. Itoh, and L. S. Vlasenko, Phys. Rev. B **78**, 153201 (2008).
[51] E. C. Reynhardt and G. L. High, J. Chem. Phys. **109**, 4090 (1998).